Journal of Energy Chemistry 25 (2016) 445–449

Contents lists available at ScienceDirect

Journal of Energy Chemistry

journal homepage: www.elsevier.com/locate/jechem

http://www.journals.elsevier.com/journal-of-energy-chemistry/

SnO_2 nanospheres among GO and SWNTs networks as anode for enhanced lithium storage performances☆

Weiwei Wen[a], Mingzhong Zou[a], Qian Feng[a], Jiaxin Li[b,*], Heng Lai[a], Zhigao Huang[a,**]

[a] College of Physics and Energy, Fujian Normal University, and Fujian Provincial Key Laboratory of Quantum Manipulation and New Energy Materials, Fuzhou 350007, Fujian, China

[b] Fujian Institute of Research on the Structure of Matter, Chinese Academy of Sciences, Fuzhou 350002, Fujian, China

ARTICLE INFO

Article history:
Received 26 September 2015
Revised 6 November 2015
Accepted 11 November 2015
Available online 22 February 2016

Keywords:
Lithium batteries
SnO_2-GO-SWNT anodes
Electrochemical performance
Energy storage

ABSTRACT

Conducting supporters of purified single-walled carbon nanotubes (SWNTs) and graphene oxide (GO) were used to confine pomegranate-structured SnO_2 nanospheres for forming SnO_2-GO-SWNT composites. As anode material for lithium ion batteries (LIBs), this composite exhibits a stable and large reversible capacity together with an excellent rate capability. In addition, an analysis of the AC impedance spectroscopy has been used to confirm the enhanced mechanism for LIB performance. The improved electrochemical performance should be ascribed greatly to the reinforced synergistic effects between GO and SWNT networks, and their enhanced contribution of the conductivity. These results indicate that this composite has potential for utilization in high-rate and durable LIBs.

1. Introduction

To meet the increasing demand of high-power lithium-ion batteries (LIBs), metal oxides as anodes with high specific capacities have attracted great attention [1,2]. Especially, SnO_2 has been considered as a potential anode material because of its high theoretical capacity of 782 mAh/g, which is much larger than that of 372 mAh/g for commercial anode of graphite [3–6]. However, similar to the other metal oxide anodes, SnO_2 anodes with low intrinsic electric conductivity and large volume changes during cycling lead to the poor stability of repetitive cycling. To overcome above mentioned limitations is important to improve the electrochemical performance of SnO_2 anodes [7–9].

Typically, electrodes were fabricated from mixtures of active materials, conductive agent of particle-shape of carbon black and polymeric binders. In this case, ion and electron transport networks were constructed only based on the point-to-point contact. The as-formed conductive networks may be destroyed quickly because of the large volume change of metal oxides during cycling. The simplest strategy is to replace the particle-shape conductive agent with carbon nanotubes (CNTs) or graphene [10]. Conducting agent of CNTs can only effectively improve their conductance based on the so-called line-to-line contact, but not effectively cushion their huge volume changes and further retain the electrode integrity. On the other hand, graphene was recently considered as a potential alternative based on surface-to-surface contact due to its high surface area, chemical tolerance and structural flexibility [11]. However, there is only a fast electron transfer within a single graphene nanosheet, while the poor electronic contacts present in active material agglomerates coated in graphene sheet. Thus, the utilization of CNTs combined with physically separated graphene is promising to accommodate the poor conductivity and volume change of metal oxides. Many kinds of anode materials consisting of CNTs, graphene and active materials have been prepared and used in LIBs to take advantage of their superior electrical conductivity and mechanical flexibility, such as TiO_2, Fe_3O_4 and MoS_2, and so forth [12–14]. Especially, Zhang et al. synthesized an anode material of SnO_2-graphene-CNT mixture for LIBs, which delivered enhanced LIB performance [15]. Therefore, the research of metal oxide anodes mixed with CNTs and /or graphene for LIBs are far from complete.

In our previous work, the purified single-walled carbon nanotubes (SWNTs) as webs of curved nanotubes can form strong intertwined entanglements with a network structure, and further afford an obviously enhanced conductivity for their composites [16,17]. Meanwhile, the MWNTs with noodle structured networks cannot effectively build up the high conducted supporters for further improve their LIB performance. The other reports also support this point of view for the SWNTs [17,18]. More importantly, using

☆ This work was supported by the Natural Science Foundations of China (No. 21203025, 51202031, 11004032 and 11074039), and Funds of Education Committee of Fujian Province (JK2013010 and JA13064).

* Corresponding author. Tel: +86 591 22867577; Fax: +86 591 22867577.
** Corresponding author.
E-mail addresses: ljx@fjirsm.ac.cn (J. Li), zghuang@fjnu.edu.cn (Z. Huang).

http://dx.doi.org/10.1016/j.jechem.2016.02.006
2095-4956/

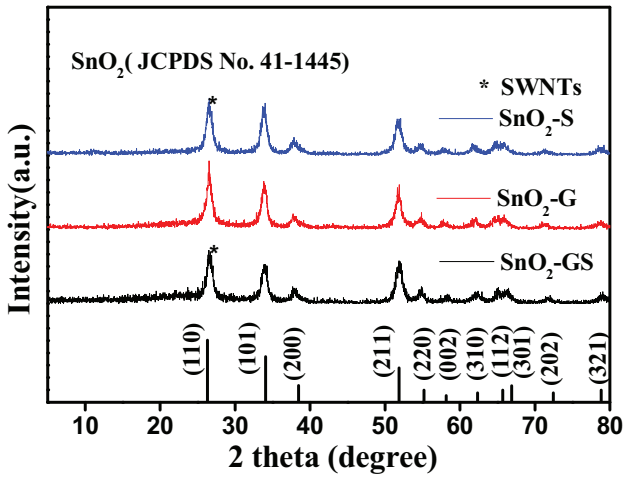

Fig. 1. XRD patterns of SnO_2-GS, SnO_2-G and SnO_2-S composites.

of both SWNTs and graphene oxide (GO) for enhancing their LIB performance has been rarely reported. Therefore, to obtain SnO_2-graphene-SWNT mixtures and investigate their enhanced LIB performance is needed.

In this work, pomegranate-structured SnO_2 nanospheres have been synthesized by a simple hydrothermal reaction and mixed with SWNTs and GO for forming composites of SnO_2-GO-SWNTs (denoted as SnO_2-GS). Directly used as electrodes via mixing with binder, the SnO_2-GS electrodes can deliver an obviously better electrochemical performance compared to the SnO_2-GO and SnO_2-SWNTs samples. In addition, an analysis of the AC impedance spectroscopy confirms that such configuration can effectively enhance the conductance of electrodes and further improve their LIB performance.

2. Experimental

2.1. Materials synthesis

All chemicals in this work were of analytical grade and used as received. GO was synthesized by the oxidation of natural flake graphite power using a modified Hummers method [16]. The SWNTs were produced by an arc-discharge method according to our previous report [17]. Pomegranate-structured SnO_2 nanospheres were prepared via a simple hydrothermal reaction. 10 mmol sodium stannate (Na_2SnO_3) was dissolved in 50 mL of 1 M glucose aqueous solutions. The clear solution was obtained through ultrasonic dispersion for 1 h before being transferred to a Telflon-lined stainless steel autoclave heated at 180 °C for 4 h. The precipitates were harvested by centrifugation and washed thoroughly with deionized water and ethanol several times, respectively. After drying at 80 °C overnight, SnO_2 powders were obtained at 550 °C for 4 h with a heating rate of 2 °C/min under air. Then, 15 mg of SWNTs was dispersed into a 30 mL GO (0.5 mg/mL) aqueous suspension by sonication for 12 h. Afterward, 70 mg of SnO_2 powders was added into above suspension through ultrasonic dispersion for 2 h. The SnO_2-GS anodes were obtained after filtrated and dried at 80 °C under vacuum. SnO_2 anode with GO as a conductive agent composites (SnO_2-G) and with SWNTs (SnO_2-S) composites were harvested in the same way.

2.2. Materials characterization

The samples were characterized by X-ray diffraction (XRD, RIGAKU SCXmini), scanning electron microscope (SEM, Hitachi SU8010), transmission electron microscope (TEM, Tecnai G2 F20).

2.3. Electrochemical measurements

The electrochemical behaviors were carried out via CR2025 coin-type cells assembled in a dry argon-filled glove box. The test cell consisted of working electrode (about 1.2–1.5 mg/cm^2) and lithium sheet which were separated by a Celgard 2300 membrane and electrolyte of 1 M $LiPF_6$ in EC:EMC:DMC (1:1:1 in volume). The working electrodes were prepared by mixing 90 wt% composites material (SnO_2-GS), and 10 wt% polymer binder (Carboxymethylcellulose, Na-CMC). The electrodes were dried at 80 °C overnight in a vacuum. These electrochemical properties are all calculated based on the overall mass of composites material. The cells were cycled by LAND2001A at room temperature. Cyclic voltammetry curves (CVs) were carried out on a CHI660D

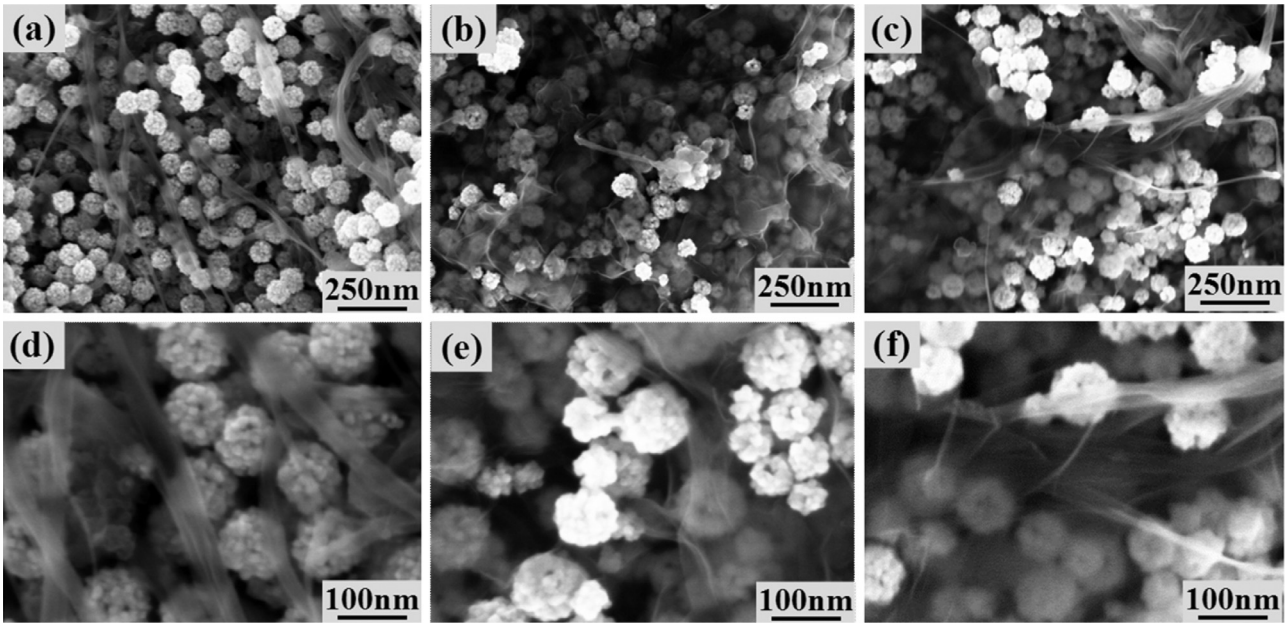

Fig. 2. SEM images of the (a,d) SnO_2-S, (b,e) SnO_2-G and (c,f) SnO_2-GS.

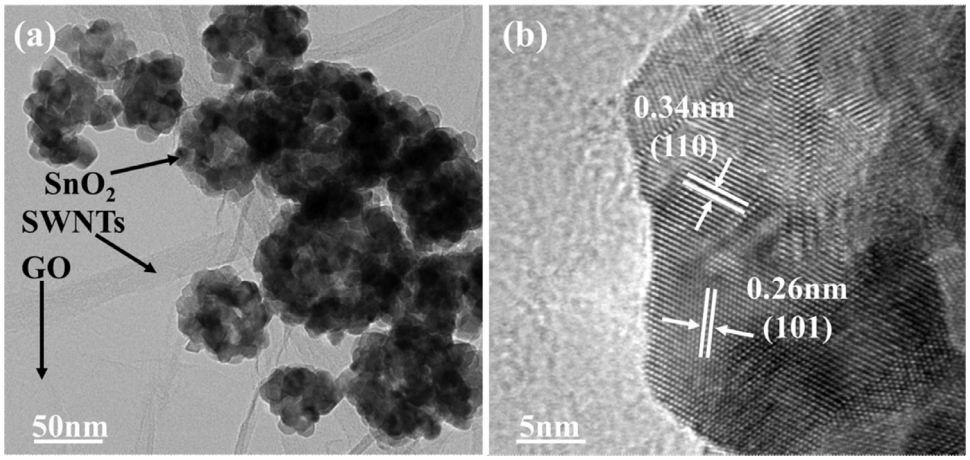

Fig. 3. TEM and the corresponding HR-TEM images of the SnO_2-GS composites.

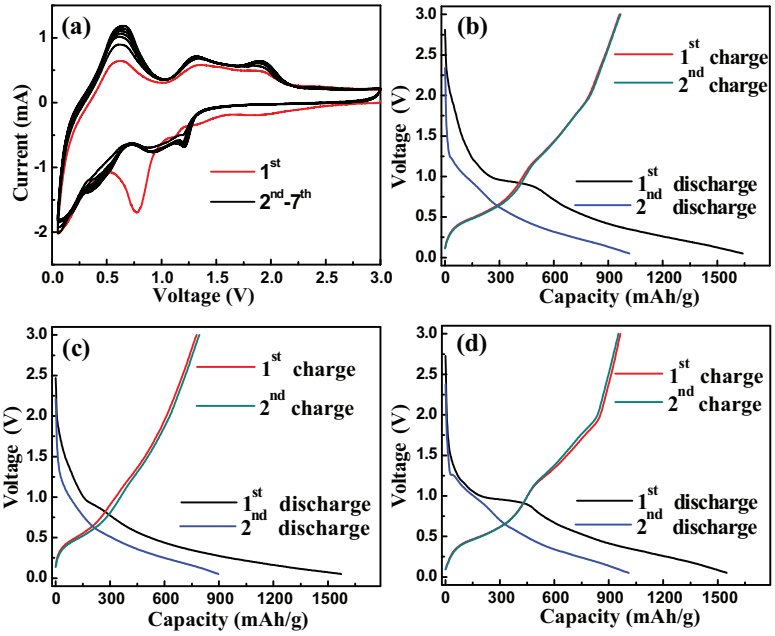

Fig. 4. Cyclic voltammetry curves of SnO_2-GS (a) and first two discharge-charge curves of SnO_2-G (b), SnO_2-S (c) and SnO_2-GS (d) electrodes between 0.05 and 3.0 V of Li insertion/extraction into/from these electrodes.

Electrochemical Workstation with a scan rate of 0.5 mV/s. Electrochemical impedance measurements were tested by the frequency ranging from 1 mHz to 100 kHz with applying an ac voltage of 5 mV.

3. Results and discussion

The XRD patterns for the SnO_2-GS, SnO_2-G and SnO_2-S are shown in Fig. 1. From Fig. 1, the three major peaks at $2\theta = 26.6^o$, 33.9^o, and 51.8^o presented in all samples are well assigned to the reflections of (110), (101) and (211) planes of tetragonal SnO_2 structure (JCPDS no. 41–1445), respectively. The clear diffraction patterns indicate the strong crystalline nature of the SnO_2 nanospheres. In addition, the diffraction peak of SWNTs near 26.5 degree was almost overlapped with the (110) plane of the SnO_2 in the composites.

Fig. 2 shows the typical SEM images of the SnO_2-S, SnO_2-G and SnO_2-GS composites recorded at different magnifications. SEM images of the SnO_2-S shown in Fig. 2(a) and (d) reveal that the SnO_2 are uniform spherical morphology, and nanospheres have a regular diameter size in the range of 90–110 nm. It is also observed that the SnO_2 nanospheres are composed of many smaller nanoparticles with a diameter of ~8 nm. In addition, the intertwined SWNTs are wrapped around the SnO_2 nanospheres, indicating a good connection between SnO_2 nanospheres and SWNT networks. Hereby, the SWNT networks can provide a good electronic conductivity between SnO_2 nanospheres. Meanwhile, the highly homogeneous distribution of GO sheets can be found in SEM images shown in Fig. 2(b) and (e). After mixing with SWNTs and GO sheets simultaneously, the different magnified SEM images of Fig. 2(c) and (f) discover that most SnO_2 nanospheres uniformly attached to or embedded within the SWNT networks and GO sheets. Such structures based on line-to-line and surface-to-surface contact between SnO_2 nanospheres and carbon of electronically conductive agents, can effectively improve their conductance and cushion their huge volume changes and further retain the electrode integrity.

To further observe the morphology and structure features, the SnO_2-GS composites have been characterized by TEM and HR-TEM. As described in Fig. 3(a) and (b), SnO_2 nanospheres keep the solid sphere structure with good nanocrystallites. Similar to our previous

report, the SWNTs appear as bundles with some appearing as individuals. As a comparison, the stacking GO sheets exhibited with an electron translucent state can be found. From Fig. 3(b), the well-defined lattice fringes with spacing of 0.34 nm and 0.26 nm correspond to the (110) and (101) planes of SnO_2, respectively.

To evaluate the electrochemical reactivity of the SnO_2-GS composites, Fig. 4(a) shows the first seven cyclic voltammetry (CV) curves of the composites between 0.05 and 3.0 V at the rate of 0.50 mV/s. During the first cathodic scan, an irreversible reduction peak of 0.75 V is assigned to the possible formation of a solid electrolyte interphase (SEI) layer and the reduction of Sn^{4+} to metallic Sn [19,20]. The intense peak from 0.5 to 0.05 V corresponds to the formation of a series of Li-Sn alloy and the Li ions intercalate in GO and SWNTs, as described in equation of $SnO_2 + 4Li^+ + 4e^- \rightarrow Sn + 2Li_2O$. In the first anodic scan, the oxidation peak appearing at 0.6 V is attribution to the de-alloying process of Li-Sn alloy in equation of $SnO_2 + 4Li^+ + 4e^- \rightarrow Sn + 2Li_2O$ and 1.30 V in the charge CVs indicates the oxidation of Sn to SnO_2, implying that equation of $SnO_2 + 4Li^+ + 4e^- \rightarrow Sn + 2Li_2O$ is reversible. From the 2nd cycle, the 0.75 V reduction peak disappear in the subsequent cycles, indicating that formation of the SEI layer only takes place during the 1st cycle. Meanwhile, the repeated Li ions insertion/extraction in/out SnO_2-GS composite at the corresponding redox peaks, respectively. In addition, Fig. 4(a) shows that the redox peaks in the following 6 cycles are very close to the 2nd one, which exhibits good reproducibility and similar shapes, revealing a good electrochemical stability for SnO_2-GS anode. Accordingly, the first two discharge-charge (D-C) voltage profiles of the SnO_2-G, SnO_2-S, and SnO_2-GS electrodes are shown in Fig. 4(b)–(d). The related potential plateaus at such as 0.60, 0.75 and 1.30 V in the D-C process are consistent with the results of CVs.

The cycling performance of SnO_2-S, SnO_2-G and SnO_2-GS electrodes in the voltage range of 0.05–3.0 V is displayed in Fig. 5. Fig. 5(a) compares the cycling performance of these three composites at 200 mA/g. The SnO_2-S, SnO_2-G and SnO_2-GS electrodes exhibit reversible capacities of 460, 520 and 760 mAh/g after 50 cycles, respectively. Apparently, the SnO_2-GS electrode exhibited a significantly improved cyclic capacity. Similarly, the SnO_2-S, SnO_2-G and SnO_2-GS electrodes were cycled under a relatively high current density of 600 mA/g after being activated at 200 mA/g in the first three cycles. As shown in Fig. 5(b), the reversible capacity of SnO_2-GS electrode can maintain a larger reversible capacity than the other two electrodes. In addition to the enhanced electrochemical stability, the rate performance of SnO_2-GS was also tested by changing the current density. As presented in Fig. 5(c), the specific capacities of SnO_2-GS were 990, 860, 760, 670 and 590 mAh/g when cycled under the current densities of 200, 400, 600, 800 and 1000 mA/g, respectively. When the current density is turned back to 200 mA/g after 50 cycles, SnO_2-GS electrode also show high reversible capacity of 780 mA h/g and retain for 60 cycles. As expected, the capacities of SnO_2-S and SnO_2-G cycled at different rates progressively decreased with cycling and obviously delivered lower capacities than that of SnO_2-GS electrode. Thus, the introduction of GO and SWNTs in SnO_2-GS hybrids can not only cushion their huge volume changes and retain the electrode integrity, but also greatly reduce the charge transfer resistance by providing an additional electron transport path to construct electronic conductive networks. The following electrochemical impedance spectroscopy (EIS) result also support this suggestion.

To further explain the electrochemical improvements on SnO_2-GS electrode, EIS was performed to identify the variations of impedance in SnO_2-S, SnO_2-G and SnO_2-GS electrodes. The Nyquist plots obtained after long cycle of these electrodes are shown in Fig. 6. As illustrated, a high-frequency semicircle and a large arc in the middle and low frequency are observed in SnO_2-S, SnO_2-G and SnO_2-GS electrodes. The equivalent circuit model of the

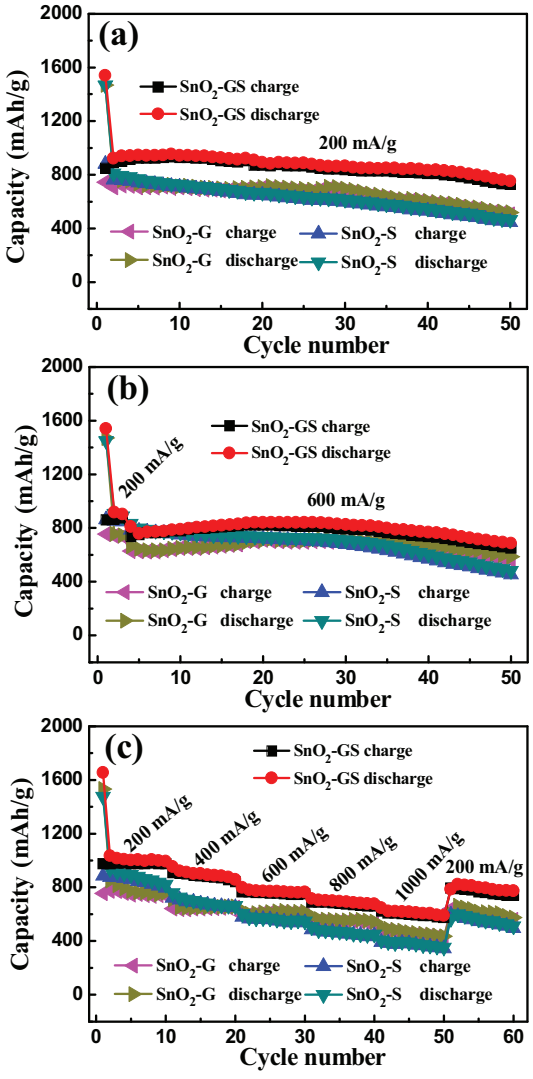

Fig. 5. Cycling performance of SnO_2-S, SnO_2-G and SnO_2-GS electrodes at room temperature: (a) at a current density of 200 mA/g, (b) at a large current density of 600 mA/g, (c) rate cycling.

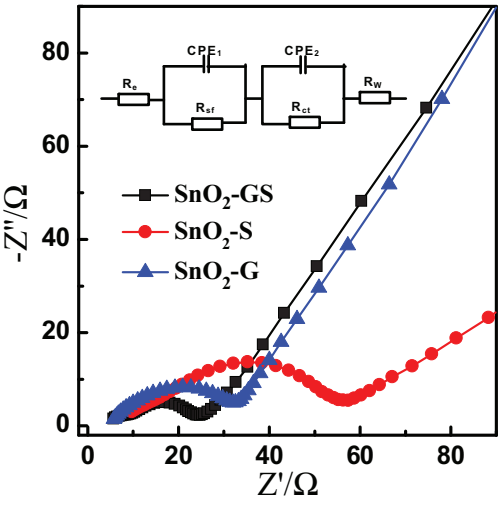

Fig. 6. Electrochemical impedance spectra of SnO_2-S, SnO_2-G and SnO_2-GS electrodes after long tested.

Table 1. Impedance parameters of SnO_2-S, SnO_2-G and SnO_2-GS anodes after test.

Samples	R_e	R_{sf}	R_{ct}
SnO_2-S	9.9	10.3	32.6
SnO_2-G	5.6	10.4	22.0
SnO_2-GS	5.5	4.6	10.8

electrode system is also shown in set of Fig. 6. The semicircle in the high-frequency region is contributed to the resistance of the Li^+ ions through the stable SEI film, and the semicircle in the middle-frequency region is associated with surface charge transfer resistance, where R_e corresponds to internal resistance; R_{sf} and C_{PE1} stand for the resistance and double-layer capacitance of the SEI layer; R_{ct} and C_{PE2} represent the charge transfer resistance and double-layer capacitance; and R_w denotes the Warburg impedance directly related to lithium ion diffusion resistance [18]. As shown in Table 1, the fitting results of R_e, R_{sf} and R_{ct} of three samples indicate that the R_{sf} and R_{ct} values of SnO_2-GS electrodes are smaller than those of SnO_2-S and SnO_2-G electrodes, indicating that the simultaneous presence of GO and SWNTs can significantly improve the resistance of the SEI layer and the charge transfer resistance for electrodes.

4. Conclusions

In summary, composites of pomegranate-structured SnO_2 nanospheres mixed with GO and SWNTs with unique nanostructure has been fabricated via a facile method. This composite used as anode for LIBs can deliver high reversible capacities of 780 and 700 mAh/g cycled at 200 and 600 mA/g after 50 cycles and good rate capability. The superior performance could be mainly attributed to the synergistic effects of the conductance contribution of GO and SWNT supporters and the stability of restricted SnO_2 nanospheres. Thus, use GO and SWNT supportors supplied a promising route to obtain SnO_2 based anode in order to achieve high-performance LIBs.

References

[1] M. Armand, J.M. Tarascon, Nature 451 (2008) 652–657.
[2] Z.Y. Wang, L. Zhou, X.W. Lou, Adv. Mater 24 (2012) 1903–1911.
[3] H. Wang, A.L. Rogach, Chem. Mater 26 (2014) 123–133.
[4] J.S. Chen, X.W. Lou, Small 9 (2013) 1877–1893.
[5] F. Wang, X.P. Song, G. Yao, M.S. Zhao, R. Liu, M.W. Xu, Z.B. Sun, Scripta. Materialia 66 (2012) 562–565.
[6] M.Z. Zou, W.W. Wen, J.X. Li, Y.B. Lin, H. Lai, Z.G. Huang, J. Energy. Chem. 23 (2014) 513–518.
[7] L. Yuan, Z.P. Guo, K. Konstantinov, H.K. Liu, S.X. Dou, J. Power. Sources 159 (2006) 345–348.
[8] F.M. Courtel, E.A. Baranova, Y. Abu-Lebdeh, I.J. Davidson, J. Power, Sources 195 (2010) 2355–2361.
[9] M.W. Xu, M.S. Zhao, F. Wang, W. Guan, S. Yang, X.P. Song, Mater. Lett 64 (2010) 921–923.
[10] S.L. Chou, Y. Zhao, J.Z. Wang, Z.X. Chen, H.K. Liu, S.X. Dou, J. Phys. Chem. C. 114 (2010) 15862–15867.
[11] B. Luo, B. Wang, X.L. Li, Y.Y. Jia, M.H. Liang, L.J. Zhi, Adv. Mater 24 (2012) 3538–3543.
[12] L.S. Zhang, W. Fan, T.X. Liu, RSC Adv. 5 (2015) 43130–43140.
[13] L.F. Shen, X.G. Zhang, H.S. Li, C.Z. Yuan, G.Z. Cao, J. Phys. Chem. L 2 (2011) 3096–3101.
[14] X.L. Jia, Z. Chen, X. Cui, Y.T. Peng, X.L. Wang, G. Wang, F. Wei, Y. Lu, ACS Nano 6 (2012) 9911–9919.
[15] B. Zhang, Q.B. Zheng, Z.D. Huang, S.W. Oh, J.K. Kim, Carbon 49 (2011) 4524–4534.
[16] W.S. Hummers, R.E. Offeman, J. Am. Chem. Soc. 80 (1958) 1339.
[17] J.X. Li, Y. Zhao, L.H. Guan, Electrochem. Comm. 12 (2010) 592–595.
[18] J.X. Li, M.Z. Zou, Y. Zhao, Y.B. Lin, H. Lai, L.H. Guan, Z.G. Huang, Electrochimica Acta. 111 (2013) 165–171.
[19] W.L. Wu, Y. Zhao, J.X. Li, C.Y. Wu, L.H. Guan, J. Energy. Chem. 23 (2014) 376–382.
[20] M.Z. Zou, W.W. Wen, J.X. Li, Y.B. Lin, H. Lai, Z.G. Huang, Mater. Res. Bul. 60 (2014) 868–871.